Acta Biologica Szegediensis

Volume 69(1):1-18, 2025
Acta Biologica Szegediensis
http://abs.bibl.u-szeged.hu/index.php/abs
DOI:10.14232/abs.2025.1.1-18

ARTICLE

ADMET and *in silico* profiling: predicting lead compounds targeting *Mycobacterium abscessus* isocitrate lyase

Mistu Karmakar, Saubashya Sur*

Postgraduate Department of Botany, Life Sciences Block, Ramananda College, Bishnupur-722122, West Bengal, India

ABSTRACT *Mycobacterium abscessus* infections exacerbate lung conditions in individuals with cystic fibrosis, bronchiectasis, or low immunity. The existing treatment options are unreliable, owing to the high antibiotic resistance of the bacterium. Isocitrate lyase is an important enzyme in mycobacteria linked with the glyoxylate cycle, facilitating persistent infections within the host. Isocitrate lyase is considered a promising drug target because its inhibition diminishes mycobacterial growth and persistence. The dearth of effective treatment highlighted the need for in silico screening for antimicrobials with improved efficacy and safety. Through literature review, ADMET profiling, and molecular docking, eight natural products were shortlisted based on drug-like properties and Lipinski's rule. AlphaFold generated high-quality structures of isocitrate lyase. Subsequently, the docking of the eight compounds with the 3D structures of isocitrate lyase was carried out. Binding energies ranged from –5.2 to –8.8 kcal/mol, with bonianic acid A and demethoxycurcumin showing the strongest affinities (–8.8 and –8 kcal/mol) against *M. abscessus* subsp. *bolletii* BD and *M. abscessus* subsp. *abscessus* ATCC 19977. Bisdemethoxycurcumin exhibited a –7.9 kcal/mol binding energy with *M. abscessus* subsp. *abscessus* ATCC 19977. Normal mode analysis confirmed their robustness. These findings support further exploration of bonianic acid A, demethoxycurcumin, and bisdemethoxycurcumin targeting isocitrate lyase, paving the way for future in vitro and in vivo studies.
Acta Biol Szeged 69(1):1-18 (2025)

KEY WORDS
ADMET
artificial intelligence
isocitrate lyase
molecular docking
Mycobacterium abscessus
natural products

ARTICLE INFORMATION
Submitted
19 August 2025
Accepted
03 November 2025
***Corresponding author**
E-mail: saubashya@gmail.com

Introduction

Mycobacteria are a diverse group of aerobic, non-motile bacteria within the phylum Actinomycota, causing wide-ranging diseases in humans and animals (Ripoll et al. 2009; Sur et al. 2023). *Mycobacterium abscessus* is a clinically significant, multidrug-resistant, non-tuberculous mycobacterium responsible for pulmonary infections in immunocompromised patients (Davidson 2018; Johansen et al. 2020; Karmakar and Sur 2025). There are three distinct subspecies of *M. abscessus*. These are *M. abscessus* subsp. *abscessus, M. abscessus* subsp. *bolletii*, and *M. abscessus* subsp. *massiliense,* respectively (Mougari et al. 2014; Zhang et al. 2024). These subspecies have been accountable for multiple clinical outbreaks of pulmonary infections worldwide and demonstrate varying levels of drug susceptibility (Bryant et al. 2016; Davidson 2018; Johansen et al. 2020). Furthermore, the intrinsic and acquired antibiotic resistance of *M. abscessus* has baffled researchers for a long time (Jarand et al. 2011; Sur et al. 2023).

Pathogenic microorganisms require carbon substrates for replication and survival within the hosts (Soni et al. 2024). Multiple lines of evidence indicate that during infection, mycobacteria utilise fatty acids instead of carbohydrates (Lee et al. 2015; Soni et al. 2024). Moreover, various glycolytic enzymes are critical for the persistence of mycobacteria within the host (Sassetti and Rubin 2003). Isocitrate lyase, associated with the glyoxylate cycle, plays a key role in bacterial pathogenicity, and its inhibition is lethal for the bacteria (Vereecke et al. 2002; Lee et al. 2015; Soni et al. 2024). Under the conditions of nutrient scarcity and suppression of TCA cycle enzymes, bacteria depend upon the glyoxylate cycle for reloading TCA cycle intermediates (Wayne and Lin 1982). The glyoxylate cycle enables the biosynthesis of cell constituents. In the glyoxylate cycle, isocitrate lyase catalyses the reversible cleavage of isocitrate to glyoxylate and succinate, while malate synthase converts glyoxylate into malate (Soni et al. 2024). Isocitrate lyase is an important enzyme linked to virulence in *M. abscessus* (Karmakar and Sur 2025) and has been a drug target (Dunn et al. 2009).

Finding appropriate treatment for infections caused by *M. abscessus* has raised apprehensions. The high antibiotic resistance of *M. abscessus* and the absence of effective

vaccines (Sur et al. 2023) have underscored the need to thwart *M. abscessus* mediated diseases from a different perspective. Even though modern medicine has surpassed traditional medicine in treating bacterial diseases, using natural products for treating diseases dates back to ancient times (Mandal et al. 2024). The interest in using natural products to prevent diseases has gained traction in developed countries, and pharmaceutical companies are increasingly investing in research and development activities (Mandal et al. 2024). Since the 1980s, researchers have identified a significant number of natural products with distinct chemotypic properties that have the potential to combat various diseases (Newman and Cragg 2020). This has provided valuable insights into natural product-based drug discovery. Technological advancements in bioinformatics and computational chemistry over the last two decades have accelerated in silico studies aimed at designing drug compounds (Ibrahim et al. 2020; Başar et al. 2024). This has saved costs and time and sparked interest in investigating natural products as a source of drugs (Başar et al. 2024). The use of computational methods in drug design has been instrumental in shaping the effectiveness of drug discovery (Bultum et al. 2022). Screening of bioactive compounds, molecular modelling, molecular docking simulations, and ADMET profiling have been successful in fast-tracking drug discovery against many diseases (Campillos et al. 2008; Dubus et al. 2009; Dong et al. 2018; Bultum et al. 2022; Ganapathy and Dick 2022).

Inhibitors of isocitrate lyase may block mycobacterial growth by impairing intracellular replication and promoting bacterial clearance from the lungs (Lee et al. 2015). There is a dearth of research on targeting isocitrate lyase from *M. abscessus* using natural compounds compared to other bacteria. In this context, this pilot study aimed at screening, ADMET profiling, molecular docking, and simulation analysis of natural compounds from existing literature that may act as lead compounds to target isocitrate lyase from *M. abscessus*. Given the clinical relevance of *M. abscessus*, the outcome of this silico study is likely to aid in the discovery of drugs to block the function of isocitrate lyase. Moreover, it would form the basis for larger studies.

Materials and methods

Retrieval of the protein sequences of isocitrate lyase

The sequences of *M. abscessus* subsp. *abscessus* ATCC 19977 (NCBI RefSeq assembly: GCF_000069185.1), *M. abscessus* subsp. *bolletii* BD (NCBI RefSeq assembly: GCF_003609715.1), and *M. abscessus* subsp. *massiliense* str GO 06 (NCBI RefSeq assembly: GCF_000277775.2) were obtained from the NCBI database (https://www.ncbi.nlm.nih.gov/data-hub/genome/) in July 2024. This pilot-scale study focused on these organisms since they are clinically significant, antibiotic resistant, and have been linked to widespread outbreaks of infections (Davidson et al. 2013; Davidson et al. 2014; Bryant et al. 2016; Sur et al. 2023). The protein sequences of the isocitrate lyases from these organisms were used for the study.

Selection of the natural products and retrieval of their structures

A literature search was carried out in July 2024 to explore natural products that have an inhibitory effect on mycobacterial proteins. The structures of the natural products were obtained from the PubChem (Kim et al. 2016) database.

Assessment of the primary sequence and prediction of the secondary, three-dimensional structure of isocitrate lyase

The primary sequence of the isocitrate lyase proteins from the studied organisms was assessed using ExPaSy ProtParam software (Gasteiger et al. 2005). The secondary structure of the isocitrate lyase was determined using the PSIPRED tool (McGuffin et al. 2000). Subsequently, using the artificial intelligence-based AlphaFold server, end-to-end modelling of the isocitrate lyase proteins was carried out to predict the three-dimensional (3D) structure (https://deepmind.google/technologies/alphafold/alphafold-server/). The 3D structures of isocitrate lyase were refined using SPDB viewer, and quality estimation of the refined structures was performed with ProSA-web (Wiederstein and Sippl 2007), ProQ (Wallner and Elofsson 2003), and SAVES (https://servicesn.mbi.ucla.edu/SAVES/), respectively. The 3D structures were visualised using PyMol (https://www.pymol.org/).

Screening of physicochemical, drug-likeness, and ADMET properties of the natural products

The selected natural products were screened for favourable physicochemical properties, drug-likeness, and ADMET (Adsorption, Distribution, Metabolism, Excretion, and Toxicity) properties using ADMETlab 3.0 (Fu et al. 2024). In this regard, the important properties were considered for the analysis. Physicochemical characteristics and drug-likeness are linked to molecular properties that influence the pharmacodynamic properties of compounds. The early assessment of ADMET properties screens out natural products with undesirable pharmacokinetic properties (Fu et al. 2024), and only those with desirable properties are considered for further analysis.

Figure 1. Three-dimensional structures of a) isocitrate lyase protein of *M. abscessus* subsp. *abscessus* ATCC 19977; b) isocitrate lyase protein of *M. abscessus* subsp. *bolletii* BD; c) isocitrate lyase protein of *M. abscessus* subsp. *massiliense* str GO 06.

Molecular docking

Molecular docking of the screened natural products and the isocitrate lyase protein was accomplished using the CB-Dock2 server (Liu et al. 2022). Protein-ligand blind docking was performed by uploading the 3D structure of the isocitrate lyase proteins and the structure of the natural products (ligand) as input. Next, the protein structures of isocitrate lyase were searched for the best cavity pockets. CB-Dock2 recognises the binding sites, computes the centre and size, and adjusts the dimensions of the docking box according to the ligand (Bultum et al. 2022; Liu et al. 2022). Subsequently, blind docking of the protein and ligand was executed with AutoDock Vina, and the docked complex was visualised and analysed.

Molecular simulation using iMODS

Molecular simulations can estimate the characteristics of docked complexes. To this end, iMODS (Lopez-Blanco et al. 2014) was utilised to explore the collective functional motion of the best protein-ligand docked complexes. This normal mode analysis (NMA) estimated the deformability factor, B-factor, eigenvalues, and variance of the docked complexes.

Results

Primary sequence analysis and physicochemical characteristics of the isocitrate lyase proteins

The isocitrate lyase protein sequences of *M. abscessus* subsp. *abscessus* ATCC 19977, *M. abscessus* subsp. *bolletii* BD, and *M. abscessus* subsp. *massiliense* str GO 06 were 430 amino acids long. The isocitrate lyase sequences of *M. abscessus* subsp. *abscessus* ATCC 19977 and *M. abscessus* subsp. *bolletii* BD, and those of *M. abscessus* subsp. *abscessus* ATCC 19977 and *M. abscessus* subsp. *massiliense* strain GO 06, displayed 99.70% sequence identity. Likewise, *M. abscessus* subsp. *bolletii* BD and *M. abscessus* subsp. *massiliense* strain GO 06 showed 100% sequence identity. Their molecular weights ranged from 46934.46 to 46948.48 daltons. These proteins displayed similar characteristics with GRAVY scores, aliphatic indexes, and isoelectric points of -0.317, 78.63, and 5.02, respectively. A low GRAVY score implied hydrophilic properties, while a high aliphatic index indicated the thermostability of the proteins. The isoelectric point divulged the acidic nature of the proteins. The instability index of the proteins ranged between 26.30 and 26.49. It specified that the proteins are stable.

Natural products used for the study

Table 1 shows the 120 natural products initially selected for the study based on the literature survey (Ibekwe and Ameh 2014; Zheng et al. 2014; Lee et al. 2015; Nguta et al. 2015; Igarashi et al. 2018; Kumar et al. 2019; Abrahams and Besra 2020; Faion et al. 2020; Baptista et al. 2021; Bosch et al. 2024; Bosshoff et al. 2024; Sirichoat et al. 2021; Knoll et al. 2022; Sullivan et al. 2022; Kumar et al. 2023; Smiejkowska et al. 2023; Acquah et al. 2024; Aina et al. 2024; Canales et al. 2024; Gagare et al. 2024; Junk et al. 2024; Kalera et al. 2024; Nyambo et al. 2024; Shahab et al. 2024; Shyam et al. 2024).

Secondary and three-dimensional structure analysis of the isocitrate lyase proteins

The secondary structure of the isocitrate lyase protein of *M. abscessus* subsp. *abscessus* ATCC 19977 had 46.74%, 8.60%, and 44.65% residues in alpha-helix, beta-strand, and coil, respectively. The percentage of alpha-helix, beta-strand, and coil in the isocitrate lyase proteins of *M. abscessus* subsp. *bolletii* BD, and *M. abscessus* subsp. *massiliense* str GO 06 were 46.51%, 8.60%, and 44.88%, correspondingly. The percentage of disordered residues in the isocitrate lyase protein across the three organisms was 5.34%.

Table 1. List of natural products screened for ADMET Profiling

Name of the natural products				
(8R,8'R,9R)-Cubebin	Andrgrapholide	Damnacanthol	Isoliquiritigenin	Pinnatin
13' – Bromo- tiliacorinine	Anthraquinone	Dehydrolupinifolinol	Isoneoratuneol	Pinocembrine
15-Acetoxyorbiculin G	Anthracene	Demethoxycurcumin	Kaempferol	Plumbagin
15-Hydroxydehydroabietic Acid	Aristolactam	Demethoxy kanugin	Khellin	Plumericin
2, -Nortiliacorinine	Artemisin	Dihydroguaiaretic acid	Knoxiadin	Quercetin
2,2-dimethyl chromenocoumarin	Artemisinin G	Diospyrin	Levofloxacin	Quinone
2'-Hydroxy-4,4',6'-trimethoxy chalcone	Atalphylline	Dimethoxyflavone	Licarin A	Rehmannioside A
25-Hydroxycycloart-23-n -3- beta-ol	Artonin	Phytol	Licarin B	Rehmannioside B
3,7-Methyljuglone	Auraptene	Ergosterol peroxide	Lupinifolin	Rubiadin
3, 3'- o- Biplumbagin	Aurisinal	Eriosemaone	Lupinifolinol	Rubiadin-1-methyl ether
3,3'-Biplumbagin	Azorellanol	Escobarine A	Lysobactin	Rumexeposide
3',4',7-Tri-O-Methylluteolin	Baicalin	Escobarine B	Mamegakinone	Salasol A
3-Epiastrapteridiol	Beilschmin A	Ethyl -p-methoxycinnamate	Maritinone	Sandaracopimeric acid
4',7-Dimethylapigenin	Bergaptol	Fargesin	Mulin-11,13-dien-20-oic acid	Scytoscalarol
4-epilarreatricin	β-sitostenone	Ferruginol	Myricetin	Selina
8,8'-Biplumbagin	Bisdemethoxycurcumin	Ferulenol	Nalidixic	Shinanolone
9,13-Epidioxy-8(14)-abieten-18-oic acid	Bonianic acid A	Flemichin	Neodiospyrin	Sorangicin
3-[4-(difluoromethyl) phenyl]-2-[(2-methylpropan-2-yl) oxycarbonylamino] propanoic acid	Carnosic acid	Galegin	Nordamnacanthal	Tiliacorinine
6-Hydroxy-16-methyl-10-(3-methylbuta-1,3-dienyl)-2-oxatetracyclo [7.5.3.01,10.03,8] heptadeca-3(8),4,6,12,16-pentaene-11,14-dione	Carpaine	Globospiramine	Obtusifoliol	Totarol
Abietane	Celahin C	Hopane - 6 Beta 11 Alpha 22, 27 -tetraol	Parguesterol	Ursolic acid
Aegicerin	Cucurbitacin E 2-O-beta-D-glucopyranoside	Hydroquinone	Parguesterol A	Valencene
Alpha curcumin	Curcumin	Icarin	Parguesterol B	Vasicine
Alpha humulene	Dalparvone	Isobavachalcone	Pectolinarin	Xanthone
Amentoflavone	Damnacanthal	Isodiospyrin	Pimaric acid	Yukocitrine

The three-dimensional structures of the isocitrate lyase proteins of *M. abscessus* subsp. *abscessus* ATCC 19977, *M. abscessus* subsp. *bolletii* BD, and *M. abscessus* subsp. *massiliense* str GO 06 (Fig. 1a-1c), modeled using the artificial intelligence-based AlphaFold server, demonstrated a very high pLDDT (predicted local distance difference test) confidence level. Furthermore, these 3D structures yielded pTM (predicted template modelling) scores of 0.97 for all the proteins. A high pTM score of 0.97 indicated that these are high-confidence structural predictions. Quality assessment of these structures, conducted after refinement, revealed the high quality of the isocitrate lyase structures. While ProSa-web analysis produced z scores -8.94, -8.75, and -8.87 for isocitrate lyases from *M. abscessus* subsp. *abscessus* ATCC 19977, *M. abscessus* subsp. *bolletii* BD, and *M. abscessus* subsp. *massiliense* str GO 06, the predicted ProQ LG scores were 7.746, 7.787, and 7.733, respectively. The outcome of ProSa-web and ProQ supported the high quality of the structures. Furthermore, examination of the Ramachandran plots demonstrated that 93.9% and 6.1% of the residues in the isocitrate lyase of *M. abscessus* subsp. *abscessus* ATCC 19977 were present in the favoured and additionally allowed regions. Similarly, for isocitrate lyase from *M. abscessus* subsp. *bolletii* BD, and *M. abscessus* subsp. *massiliense* str GO 06, the residues in the favoured and additionally allowed regions were 93.7% and 6.3%, respectively. This has been strongly supported by the RMSD (root mean square deviation) values of the C-α atoms in the 3D structures of isocitrate lyase. These were 0.15 Å between *M. abscessus* subsp. *abscessus* ATCC 19977 and *M. abscessus* subsp. *bolletii* BD; 0.16 Å between *M. abscessus* subsp. *abscessus* ATCC 19977 and *M. absces-*

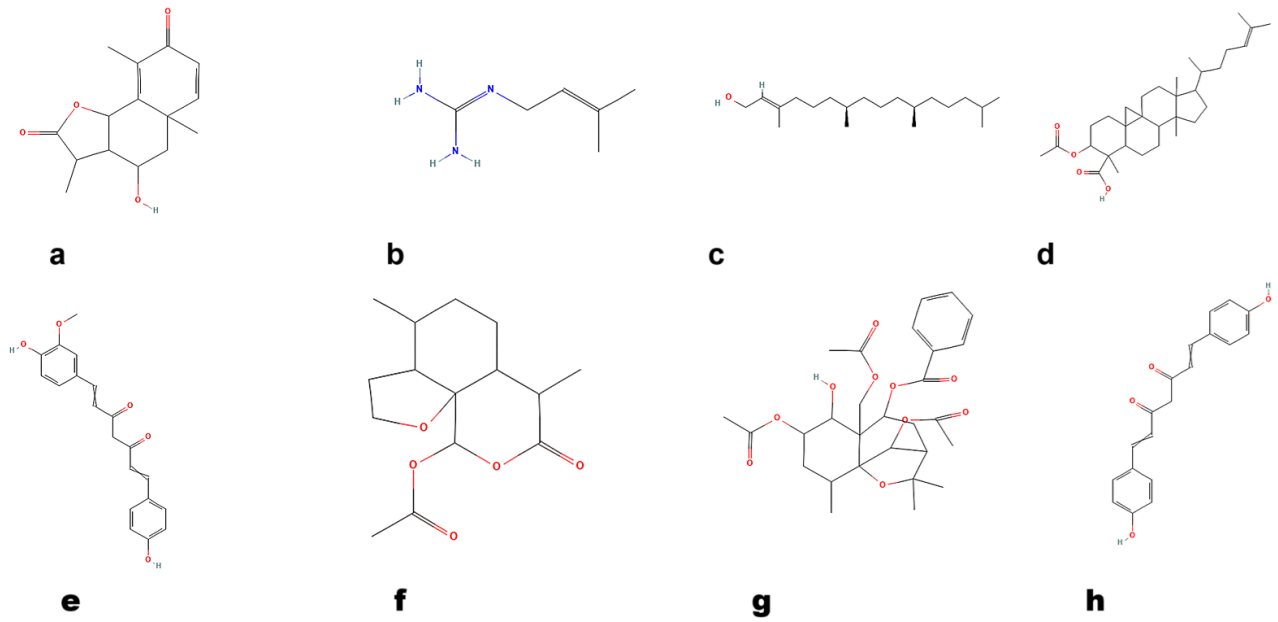

Figure 2. 2D structures of the screened natural products a) artemisin (PubChem id: 621620); b) galegin (PubChem id: 10983); c) phytol (PubChem id: 5280435); d) bonianic acid A (PubChem id: 75995918); e) demethoxycurcumin (PubChem id: 146723); f) artemisinin G (PubChem id: 73880832); g) celahin C (PubChem id: 85090205); h) bisdemethoxycurcumin (PubChem id: 147439).

sus subsp. *massiliense* str GO 06; and 0.11 Å between *M. abscessus* subsp. *bolletii* BD and *M. abscessus* subsp. *massiliense* str GO 06.

Outcome of screening natural products for desirable physicochemical, drug-likeness, and ADMET properties

The extent to which specific compounds resemble well-known pharmaceuticals based on the balance between molecular and structural characteristics is called drug-likeness (Gheidari et al. 2024). In this regard, the evaluation of physicochemical properties, pharmacophoric properties, metabolic stability, reactivity, and toxicity assumes paramount importance (Ertl et al. 2000). Additionally, Lipinski's rule aids in recognising the viability of probable drug candidates based on their solubility and permeability (Gheidari et al. 2024). The compounds flouting the rule often display inferior absorption and penetration capabilities. Moreover, ADMET profiling of compounds improves the success rate by providing insights into the pharmacological and toxicological characteristics (Gheidari et al. 2024). A comprehensive profiling of the 120 natural products using ADMETlab 3.0 identified 112 natural products with undesirable properties. These 112 natural products had the propensity to exhibit high levels of toxicity, mutagenicity, carcinogenicity, and undesirable absorption, metabolism, and excretion properties, and didn't satisfy Lipinski's rule. Additionally, their physicochemical properties were not favourable. As a result, 8 natural products out of 120 were identified to possess favourable properties that increased the likelihood of success and were finalised for consideration (Table 2). These are artemisin, galegin, phytol, bonianic acid A, demethoxycurcumin, artemisinin G, celahin C, and bisdemethoxycurcumin (Fig. 2a-2h). The predicted physicochemical, pharmacokinetic, and ADMET properties of these natural products are summarised in Table 2. A few values (precise) of these properties are identical for some of the natural products.

As far as the Lipinski's rule for these eight natural products is concerned, it was observed that celahin C (molecular weight ≈ 532.2 > 500) and bonianic acid A (logP ≈ 5.83 > 5) breached only one of the criteria of the rule. The rest of the six natural products fulfilled the criteria. Since celahin C and bonianic acid A did not violate more than one of the criteria of Lipinski's rule, they were considered favourable by ADMETlab 3.0 (Lipinski 2004; Fu et al. 2024). Hence, these eight natural products had reasonable absorption properties. The molecular weight of these compounds ranged from 127.11 to 532.23 Da, falling within the optimal range of 100-600 (Başar et al. 2024). This supported good oral bioavailability. The TPSA (Topological Polar Surface Area) values of these compounds span from 20.23 to 134.66. This being < 140 suggests excellent capability of absorption inside the intestine (Ibrahim et al. 2020). The log S values representing the water solubility of the compounds at 25 °C varied

Table 2. Predicted physicochemical, pharmacokinetic, and ADMET properties of artemisin, artemisinin G, bisdemethoxycurcumin, bonianic acid A, celahin C, demethoxycurcumin, phytol, and galegin

Properties	Artemisin	Artemisinin G	Bisdeme-thoxycur-cumin	Bonianic acid A	Celahin C	Deme-thoxycur-cumin	Phytol	Galegin
Lipinski Rule	Favorable	Favorable	Favorable	Favorable	Favorable	Favorable	Favorable	Favorable
Molecular weight	262.12	282.15	308.1	498.37	532.23	338.12	296.31	127.11
TPSA	63.6	61.83	74.6	63.6	134.66	83.83	20.23	64.4
log S	-2.761	-2.834	-3.722	-4.624	-4.169	-3.864	-6.192	-1.184
log P	0.723	1.904	2.567	5.826	2.759	2.518	7.229	1.426
log D	1.119	2.076	2.745	4.237	2.884	2.77	4.485	1.276
Absorption								
CaCo-2 Permeability	-5.1	-4.671	-4.961	-5.062	-5.15	-5.223	-4.961	-4.817
Pgp-inhibitor	0.119	0.014	0.009	0.034	0.994	0.014	0	0.018
Pgp-substrate	0.257	0.139	0.003	0	0.404	0.004	0.005	0.998
Human Intestinal Absorption (HIA)	0.046	0.019	0	0	0.005	0.001	0.002	0.04
Distribution								
Plasma protein binding (PPB)	68.397	64.561	86.998	96.678	56.171	87.96	89.449	38.184
Blood-brain barrier penetration (BBB)	0.655	0.069	0.018	0.699	0.193	0.018	0.986	0.05
Metabolism								
CYP1A2 inhibitor	0	0.993	0.057	0	0	0.581	0	0.002
CYP2C19 inhibitor	0.001	0	0.01	0	0.397	0.065	0.085	0
CYP2C9 inhibitor	0	0.001	0.782	0	0.007	0.283	0.993	0
CYP2D6 inhibitor	0	0	0.289	0	0.92	0.113	0.011	0.053
CYP3A4 inhibitor	0.681	0.002	0.972	0	0.752	0.953	0.094	0
Excretion								
CL_{plasma} (ml/min/kg)	8.852	6.259	11.515	2.483	1.998	10.216	6.818	6.12
$T_{½}$ (hours)	1.982	0.971	1.071	1.295	1.144	1.115	0.272	2.341
Toxicity								
hERG blockers	0.03	0.025	0.583	0.132	0.076	0.496	0.232	0.158
AMES mutagenicity	0.3	0.499	0.326	0.054	0.516	0.368	0.1	0.636
Carcinogenicity	0.571	0.45	0.08	0.158	0.498	0.09	0.275	0.578
Eye corrosion	0.171	0.218	0.056	0.006	0	0.054	0.996	0.021
Respiratory toxicity	0.377	0.136	0.564	0.399	0.007	0.659	0.672	0.647
Human hepatotoxicity	0.519	0.666	0.357	0.597	0.111	0.349	0.63	0.59
Drug-induced nephrotoxicity	0.226	0.606	0.085	0.207	0.262	0.157	0.145	0.161
Hematotoxicity	0.239	0.328	0.01	0.121	0.03	0.019	0.211	0.429
Genotoxicity	0.601	0.462	0.11	0.003	0.333	0.042	0	0.795

* log S: Log of aqueous solubility value, log P: Log of n-octanol/water distribution coefficient, Pgp – polyglycoprotein, CYP: Cytochrome P450. TPSA: Topological Polar Surface Area.

between -1.184 and -6.192. Except for phytol, bonianic acid A, and celahin C, others exhibited appropriate water solubility as they fell within the optimal range (-0.4 – 0.5) (Başar et al. 2024). This outcome divulged that these three compounds were moderately water-soluble. The log P (the octanol-water partition coefficient) values measure the lipophilicity of compounds, influencing the absorption, distribution, and metabolism of a drug. It was observed that, except for bonianic acid A and phytol, log P values of the other compounds were within the range of 0-3 (Başar et al. 2024). Bonianic acid A and phytol showed high lipophilicity. The assessment of log D is valuable because it offers a more accurate and pH-dependent degree of lipophilicity, which is vital for understanding the role of ionizable compounds in biological systems. The log D values of the screened compounds ranged from 1.119 to 4.485.

The utilisation of CaCo2 (Cancer coli-2) permeability data evaluates the absorption of pharmaceutical products in the human gastrointestinal tract (Gheidari et al.

2024). The seven compounds were found within the accepted range (higher than -5.15 log units), with a minor deviation in demethoxycurcumin. Plasma glycoprotein (Pgp) affects the ADMET properties of drugs, making it crucial to examine the relations between the drug and transporter proteins (Bultum et al. 2022). Among the studied compounds, celahin C divulged the strongest probability of acting as a Pgp inhibitor, whereas the remaining seven compounds displayed borderline characteristics consistent with Pgp non-inhibitor. While bonianic acid A was clearly a Pgp non-substrate, galegin showed the highest probability of being a Pgp substrate. Bisdemethoxycurcumin, demethoxycurcumin, phytol and artemisinin G exhibited borderline probability of being a Pgp non-substrate. Artemisin, and celahin C showed a low probability of being considered as Pgp substrate. The HIA (human intestinal absorption) values are categorised as excellent (0-0.3), medium (0.3-0.7) and poor (0.7-1.0) (Jaiswal and Kumar 2023). From Table 2, the values of HIA in the studied compounds demonstrate a high probability of being absorbed within the intestinal membrane. A study of plasma protein binding (PPB) is vital for estimating the therapeutic index of the drugs, and those with PPB values < 90% demonstrate enhanced therapeutic index (Gheidari et al. 2024). The study demonstrated that seven compounds exhibited a stronger therapeutic index compared to bonianic acid A. It has been reported that compounds with BBB (Blood-Brain Barrier) values below 1 do not adversely affect the central nervous system. Based on the results in Table 2, the values of BBB in all eight compounds were below 1.

Cytochrome P450s (CYPs) are heme-containing enzymes vital for xenobiotic metabolism in the body through oxidation, playing a role in detoxification (Kamel et al. 2022). Their inhibition or induction results in drug-drug interactions (Bultum et al. 2022; Kamel et al. 2022). Table 2 divulged that CYP1A2 appeared to be inhibited by artemisinin G. Bisdemethoxycurcumin, and phytol had the probability to inhibit CYP2C9. CYP3A4 was predicted to be inhibited by bisdemethoxycurcumin, celahin C, and demethoxycurcumin. Moreover, celahin C possibly inhibited CYP2D6. CYP2C19 was not inhibited by any of the eight compounds. Additionally, artemisin, bonianic acid A, and galegin did not appear to inhibit any of the tested cytochrome enzymes. Excretion is an important pharmacokinetic property associated with bioavailability and is crucial for determining the rate of drug dose for steady-state concentration (Veber et al. 2002). The CL_{plasma} penetration clearance values for the eight compounds ranged from 1.998 to 11.515, all within the acceptable limits. The $T_{1/2}$ (half-life) represents the time required for the plasma drug concentration to decrease by 50% (Fu et al. 2024). It varied from 0.272 to 2.341. Phytol had a comparatively shorter half-life than the other seven compounds.

It is necessary to evaluate the toxicity profile of potential drug compounds and assess their suitability for therapeutic applications. The prediction of various toxicity parameters using ADMET, ranging from 0 to 1, for the eight compounds, is presented in Table 2. The output value for the probability of being a hERG blocker ranged between 0 to 1. In this regard, bisdemethoxycurcumin revealed a probability value of 0.583. This was regarded as a moderate risk by ADMETlab 3.0. The remaining seven compounds did not pose any risk. The AMES mutagenicity values ranged from 0 to 1. Among the eight compounds, only galegin exhibited an elevated value. This was deemed moderate risk in ADMETlab 3.0. The remaining seven compounds did not show any mutagenic potential. Interestingly, none of the compounds was identified as carcinogenic, hematotoxic, hepatotoxic, nephrotoxic, or respiratory toxic. However, phytol exhibited the potential to cause eye corrosion. This is in contrast to the other seven compounds. The probability of being genotoxic ranged between 0 to 1. Galegin exhibited a likelihood of being genotoxic, while artemisin revealed an elevated value of 0.601. ADMETlab 3.0 considered this as moderately genotoxic. None of the remaining six compounds was genotoxic.

Molecular docking analysis reveals the effective natural products

Molecular docking was performed for computational analyses of the eight screened natural products targeting the isocitrate lyase protein from *M. abscessus* subsp. *abscessus* ATCC 19977, *M. abscessus* subsp. *bolletii* BD, and *M. abscessus* subsp. *massiliense* str GO 06. The docking results of the eight natural products, together with contact residues of the proteins linked to the binding interactions, are summarised in Table 3. It is worth noting that CB-Dock2 performs cavity sorting (based on size) after cavity determination. It is known that a larger cavity size corresponds to a higher number of functional residues, thereby increasing the potential for ligand binding interactions (Thada et al. 2020; Kumpf et al. 2021). The Vina score represented the binding energy in the potential binding sites (Liu et al. 2022). The outcome portrayed robust binding affinities of the studied compounds based on the lowest binding energy. Bisdemethoxycurcumin docked (Vina score of -7.9 kcal/mol) isocitrate lyase of *M. abscessus* subsp. *abscessus* ATCC 19977. Bisdemethoxycurcumin formed three hydrogen bonds with ALA278, ALA281, and GLN310 residues and Pi-Anion interaction with LYS344 within a cavity volume of 449 $Å^3$ (Fig. 3a-3c). The rest of the residues formed van der Waals interactions. Docking with CB-Dock 2 showed

Table 3. Output of the molecular docking of isocitrate lyase of *M. abscessus* subsp. *abscessus* ATCC19977, *M. abscessus* subsp. *bolletii* BD, *M. abscessus* subsp. *massiliense* str GO 06 with the screened natural products

Natural product	Organism	CurPocket ID	Vina score	Cavity volume (Å3)	Center (x, y, z)	Docking size (x, y, z)	Contact residues
Artemisin	*M. abscessus* subsp. *abscessus* ATCC19977	C1	-6.7	449	-18, 8, -1	19, 19, 19	Chain A: LYS24 GLY25 ILE26 ALA278 PRO279 ALA281 ASP282 ASP306 PHE307 PRO308 ASP309 GLN310 LEU311
	M. abscessus subsp. *bolletii* BD	C3	-6.7	376	19, 0, -4	19, 19, 19	Chain A: LYS24 GLY25 ILE26 ALA278 PRO279 ALA281 ASP282 PHE307 PRO308 ASP309 GLN310 LEU311
	M. abscessus subsp. *massiliense* GO 06	C2	**-6.8**	333	-2, 16, -7	19, 19, 19	Chain A: LYS24 GLY25 ILE26 ALA278 PRO279 ALA281 ASP282 PHE307 PRO308 ASP309 GLN310 LEU311
Artemisinin G	*M. abscessus* subsp. *abscessus* ATCC19977	C1	-5.7	449	-18, 8, -1	19, 19, 19	Chain A: LYS24 GLY25 THR27 PRO279 ASP306 PHE307 PRO308 ASP309 GLN310
	M. abscessus subsp. *bolletii* BD	C1	**-6**	764	2, 15, 9	26, 19, 19	Chain A: MET78 GLN81 GLN82 ARG84 ALA85 GLU382 SER385 ARG388 GLY389 TYR390
	M. abscessus subsp. *massiliense* GO 06	C1	-5.5	1154	15, -3, -8	19, 19, 19	Chain A: ILE55 ALA59 LYS62 SER66 TYR67 ILE68 LYS88 ASP146 ASN147 VAL150 PRO151
Bisdemethoxycur-cumin	*M. abscessus* subsp. *abscessus* ATCC19977	C1	**-7.9**	449	-18, 8, -1	25, 25, 25	Chain A: LYS24 GLY25 ILE26 TRP57 VAL60 SER61 LYS62 ASP63 ASP64 ASP65 ALA278 PRO279 ALA281 ASP282 LYS304 ASP309 GLN310 LEU311 GLY339 ALA340 MET341 GLY342 LYS344
	M. abscessus subsp. *bolletii* BD	C3	-7.9	376	19, 0, -4	25, 25, 25	Chain A: PRO21 LYS24 GLY25 ILE26 TRP57 THR61 ALA278 PRO279 ALA281 ASP282 ASP306 PHE307 PRO308 ASP309 GLN310 LEU311
	M. abscessus subsp. *massiliense* GO 06	C2	-7.7	333	-2, 16, -7	25, 25, 25	Chain A: PRO21 LYS24 GLY25 ILE26 TRP57 THR61 LYS62 ALA278 PRO279 ALA281 ASP282 LEU283 ASP306 PHE307 PRO308 ASP309 GLN310 LEU311
Bonianic acid A	*M. abscessus* subsp. *abscessus* ATCC19977	C1	-8.4	449	-18, 8, -1	25, 25, 25	Chain A: PRO21 LYS24 GLY25 ILE26 TRP57 VAL60 SER61 LYS62 ASP63 ASP64 ASP65 ALA281 ASP282 LYS304 PRO308 ASP309 GLN310 LEU311 GLY339 ALA340 MET341 GLY342 LYS344
	M. abscessus subsp. *bolletii* BD	C3	**-8.8**	376	19, 0, -4	25, 25, 25	Chain A: PRO21 LYS24 GLY25 TRP57 VAL60 THR61 LYS62 ASP63 ASP64 ASP65 ALA281 ASP282 LYS304 PRO308 ASP309 GLN310 LEU311 GLY339 ALA340 MET341 GLY342 LYS344
	M. abscessus subsp. *massiliense* GO 06	C2	-8.5	333	-2, 16, -7	25, 25, 25	Chain A: PRO21 ARG22 LYS24 GLY25 TRP57 VAL60 THR61 LYS62 ASP63 ASP64 ASP65 ALA281 ASP282 LYS304 PRO308 ASP309 GLN310 LEU311 GLY339 ALA340 MET341 GLY342 LYS344
Celahin C	*M. abscessus* subsp. *abscessus* ATCC19977	C2	-6.2	281	-3, 16, 17	22, 22, 22	Chain A: ASP29 TYR30 GLN34 VAL35 LEU38 ALA163 LEU164 TYR167 ILE208 ARG209 THR212 SER213 LEU216
	M. abscessus subsp. *bolletii* BD	C3	**-6.3**	376	19, 0, -4	22, 22, 22	Chain A: PRO21 ARG22 LYS24 TRP57 VAL60 THR61 LYS62 ASP63 ASP64 ASP282 LYS304 ASP309 LEU311 LYS344
	M. abscessus subsp. *massiliense* GO 06	C2	-6.3	333	-2, 16, -7	22, 22, 22	Chain A: PRO21 ARG22 LYS24 TRP57 VAL60 THR61 LYS62 ASP63 ASP64 ASP282 LYS304 PRO308 ASP309 LEU311 LYS344

Table 3. Continued

Natural product	Organism	CurPocket ID	Vina score	Cavity volume (Å3)	Center (x, y, z)	Docking size (x, y, z)	Contact residues
Demethoxycurcumin	*M. abscessus* subsp. *abscessus* ATCC19977	C1	**-8**	449	-18, 8, -1	26, 26, 26	Chain A: PRO21 LYS24 GLY25 ILE26 TRP57 SER61 LYS62 ASP63 ASP64 ASP65 ALA278 PRO279 ALA281 ASP282 LYS304 PHE307 PRO308 ASP309 GLN310 LEU311 GLY339 ALA340 MET341 GLY342 LYS344
	M. abscessus subsp. *bolletii* BD	C3	-7.9	376	19, 0, -4	26, 26, 26	Chain A: PRO21 LYS24 GLY25 ILE26 TRP57 VAL60 THR61 LYS62 ASP63 ALA278 PRO279 ALA281 ASP282 LYS304 PHE307 PRO308 ASP309 GLN310 LEU311 GLY342 LYS344
	M. abscessus subsp. *massiliense* GO 06	C2	-8	333	-2, 16, -7	26, 26, 26	Chain A: LYS24 GLY25 ILE26 TRP57 THR61 LYS62 ASP63 ASP64 ASP65 ALA278 PRO279 ALA281 ASP282 LEU283 LYS304 PHE307 ASP309 GLN310 LEU311 GLY339 ALA340 MET341 GLY342 LYS344
Phytol	*M. abscessus* subsp. *abscessus* ATCC19977	C1	**-6.2**	449	-18, 8, -1	25, 25, 25	Chain A: ARG22 LYS24 GLY25 ILE26 TRP57 SER61 ALA278 PRO279 ALA281 ASP282 PHE307 PRO308 ASP309 GLN310 LEU311
	M. abscessus subsp. *bolletii* BD	C3	-5.4	376	19, 0, -4	25, 25, 25	Chain A: PRO21 ARG22 LYS24 GLY25 ILE26 TRP57 THR61 ALA278 PRO279 ALA281 ASP282 PHE307 PRO308 ASP309 GLN310 LEU311
	M. abscessus subsp. *massiliense* GO 06	C2	-5.9	333	-2, 16, -7	25, 25, 25	Chain A: PRO21 LYS24 GLY25 ILE26 TRP57 THR61 ALA278 PRO279 ALA281 ASP282 ASP306 PHE307 PRO308 ASP309 GLN310 LEU311
Galegin	*M. abscessus* subsp. *abscessus* ATCC19977	C1	-5.2	449	-18, 8, -1	17, 17, 17	Chain A: LYS24 GLY25 ILE26 TRP57 SER61 ALA278 PRO279 TYR280 ALA281 ASP282 ASP309 GLN310 LEU311
	M. abscessus subsp. *bolletii* BD	C3	-5.3	376	19, 0, -4	17, 17, 17	Chain A: LYS24 GLY25 ILE26 TRP57 THR61 ALA278 PRO279 TYR280 ALA281 ASP282 ASP309 GLN310 LEU311
	M. abscessus subsp. *massiliense* GO 06	C2	**-5.4**	333	-2, 16, -7	17, 17, 17	Chain A: LYS24 GLY25 ILE26 TRP57 THR61 ALA278 PRO279 TYR280 ALA281 ASP282 ASP309 GLN310 LEU311

a Vina score of -8 kcal/mol for demethoxycurcumin towards isocitrate lyase of *M. abscessus* subsp. *abscessus* ATCC 19977. In this case, the cavity volume was 449 Å^3. Demethoxycurcumin exhibited three strong hydrogen bonds with residues ALA278, GLN310, and LYS344; and a non-covalent Pi-alkyl interaction with LYS344 (Fig. 4a-4c). Furthermore, it formed van der Waals interactions with other residues. The highest binding affinity, illustrated by the Vina score of -8.8 kcal/mol in a cavity volume of 376 Å^3, was observed for bonianic acid A and isocitrate lyase of *M. abscessus* subsp. *bolletii* BD. Here, LYS344 revealed a strong hydrogen bond with bonianic acid A, while the LYS24 and TRP57 residues formed Pi-alkyl non-covalent interaction (Fig. 5a-5c). Moreover, bonianic acid A displayed van der Waals interactions with other residues. Phytol showed optimal binding to isocitrate lyase of *M. abscessus* subsp. *abscessus* ATCC 19977, with a Vina score of -6.2 kcal/mol. Artemisinin G demonstrated the most prominent interaction with the active site residues of *M. abscessus* subsp. *bolletii* BD isocitrate lyase, with a Vina score of -6 kcal/mol and a cavity volume of 764 Å^3. Celahin C also established a high binding affinity to *M. abscessus* subsp. *bolletii* BD isocitrate lyase, with a Vina score of -6.3 kcal/mol. The molecular docking result portrayed artemisin and galegin as interacting with the isocitrate lyase of *M. abscessus* subsp. *massiliense* str GO 06, with Vina scores of -6.8 and -5.4 kcal/mol and cavity volumes of 333 Å^3. The docking analysis revealed that bonianic

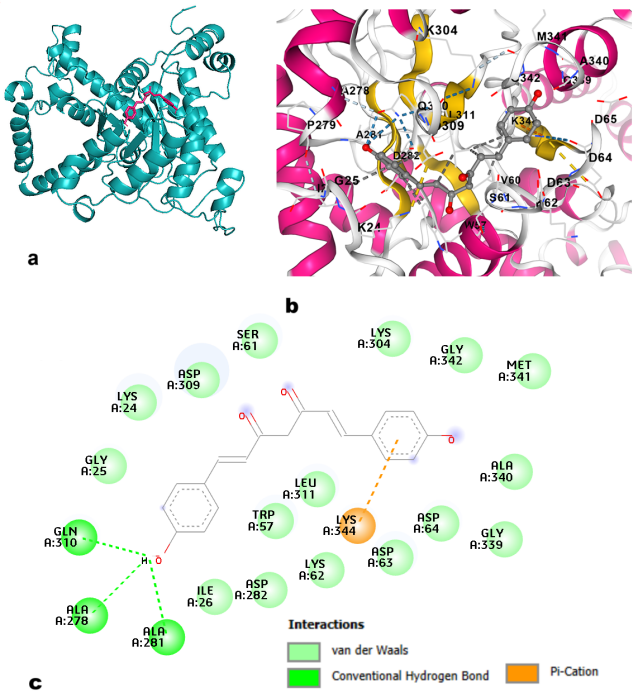

Figure 3. Molecular docking of the three-dimensional structure of the isocitrate lyase protein and bisdemethoxycurcumin. a) docked structure of the *M. abscessus* subsp. *abscessus* ATCC 19977 isocitrate lyase and bisdemethoxycurcumin (in dark pink); b) docking interactions; c) 2D details of the binding interactions.

acid A and isocitrate lyase of *M. abscessus* subsp. *bolletii* BD; demethoxycurcumin and isocitrate lyase of *M. abscessus* subsp. *abscessus* ATCC 19977; and bisdemethoxycurcumin and isocitrate lyase of *M. abscessus* subsp. *abscessus* ATCC 19977 were the top docked complexes. While the docking outcome was interesting, it may be mentioned that docking was performed on AlphaFold models without experimental complexes; therefore, active-site assignment is provisional. Future work will include re-docking of reference ligands and site validation against known catalytic residues.

Molecular simulation analysis of the top docked complexes

Molecular simulation of the top docked complexes, viz., bisdemethoxycurcumin and isocitrate lyase of *M. abscessus* subsp. *abscessus* ATCC 19977, demethoxycurcumin, and isocitrate lyase of *M. abscessus* subsp. *abscessus* ATCC 19977, and bonianic acid A and isocitrate lyase of *M. abscessus* subsp. *bolletii* BD were performed with normal mode analysis (NMA). These simulations demonstrated the stability, deformability, and motion of the atoms (Fig. 6-8). The high and low values portray flexible and rigid regions, respectively. The B-factor values (Fig. 6c, 7c, and 8c) specified how protein residues deviate from their actual position during interactions. The eigenvalues used to quantify the degree of stiffness or deformability of the docked complexes ranged from 6.890083e-05 to 7.038168e-05. Higher eigenvalues indicate stiffer collective motions, while lower eigenvalues specify more flexibility (Lopez-Blanco et al. 2014). The individual and cumulative variances in the docked complexes were visualised (Fig. 6e, 7e, and 8e), respectively. The eigenvalues and variances reflected greater energy requirements for displacing the residues from their initial positions. The covariance heatmaps (Fig. 6f, 7f, and 8f) highlighted the correlated, uncorrelated, and anticorrelated motions between dynamic regions. The red regions with high positive covariance values move in the same direction during the collective motions, while white regions, with near-zero covariance values, move independently of each other. Blue regions with high negative covariance values move in opposite

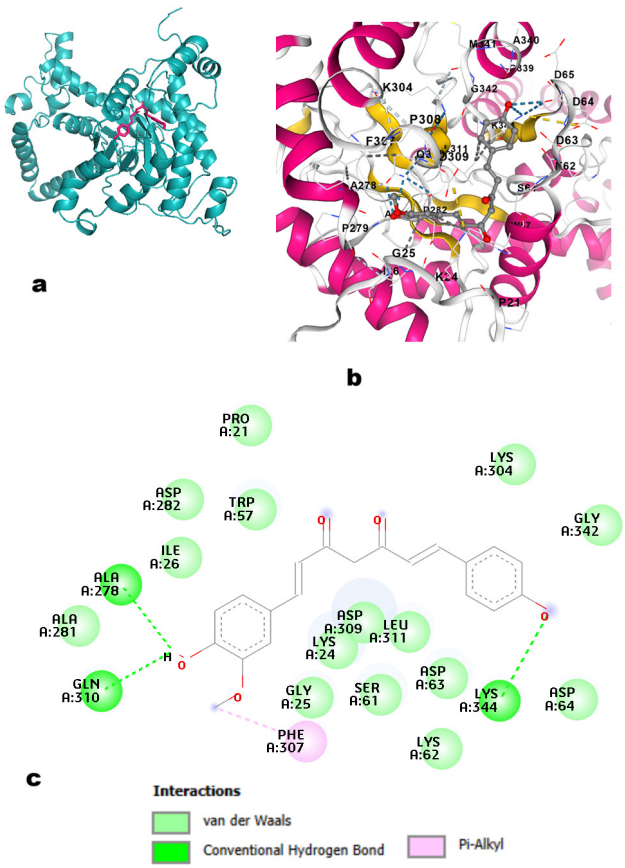

Figure 4. Molecular docking of the three-dimensional structure of the isocitrate lyase protein and demethoxycurcumin. a) docked structure of the *M. abscessus* subsp. *abscessus* ATCC 19977 isocitrate lyase and demethoxycurcumin (in dark pink); b) docking interactions; c) 2D details of the binding interactions.

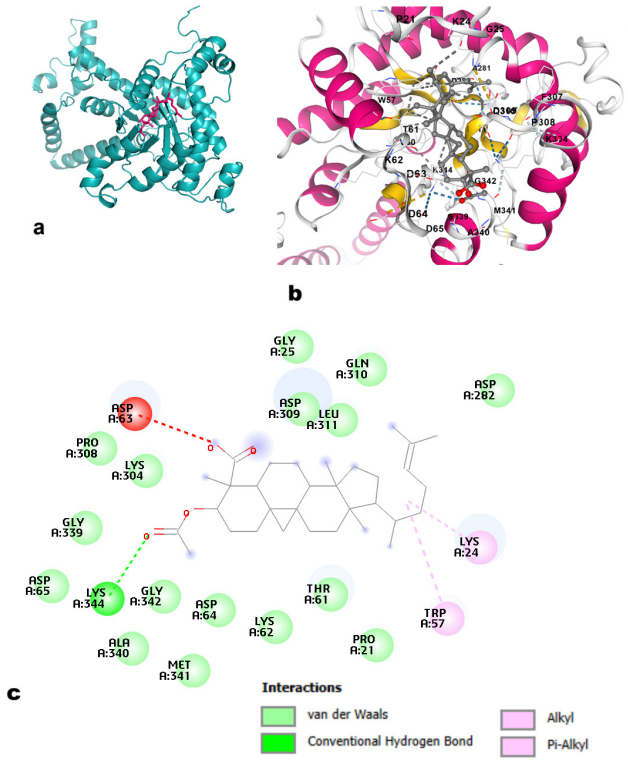

Figure 5. Molecular docking of the three-dimensional structure of the isocitrate lyase protein and bonianic acid A. a) docked structure of the *M. abscessus* subsp. *bolletii* BD isocitrate lyase and bonianic acid A (in dark pink); b) docking interactions; c) 2D details of the binding interactions.

directions. The elastic network potential of the docked complexes (Fig. 6g, 7g, and 8g) specified the relationship between atomic residues. The flexible and stiff residues are denoted by white and dark grey. The latter remains scattered in the elastic map.

Discussion

Pathogenic mycobacteria depend upon fatty acid substrates for persistence and survival during infection, and the glyoxylate cycle enables their utilisation as a carbon source (Lee et al. 2015; Soni et al. 2024). Isocitrate lyase, an important enzyme of the glyoxylate cycle (Vereecke et al. 2002), is responsible for fatty acid catabolism and virulence in mycobacteria. The absence of isocitrate lyase homologs in mammals makes it an attractive target for drug development. Inhibitors of isocitrate lyase may block mycobacterial growth (Lee et al. 2015) by impairing intracellular replication and promoting bacterial clearance from the lungs. In this regard, the exploration for appropriate inhibitors assumes significance. This bioinformatic analysis attempted to identify potential natural products that can act against isocitrate lyase in *M. abscessus*, since they can target specific biological pathways and interact with different proteins linked to various diseases (Mandal et al. 2024).

The physicochemical properties of the isocitrate lyase protein sequences of *M. abscessus* subsp. *abscessus* ATCC 19977, *M. abscessus* subsp. *bolletii* BD, and *M. abscessus* subsp. *massiliense* str GO 06 revealed that they are within the optimal range. A low GRAVY score implied hydrophilic properties, while a high aliphatic index indicated the thermostability of the proteins. The isoelectric point divulged the acidic nature of the proteins. The instability index specified that the proteins are stable. The outcome of the secondary and tertiary structure analysis of the isocitrate lyase proteins implied stability of the structures. A comparatively higher percentage of alpha-helix residues in the secondary structures enhances the stability of the protein owing to the increased stabilising hydrogen bonds and interactions between residues. Additionally, a high pTM score designates the overall quality of the predicted protein tertiary structures, signifying that the predicted structure is likely to be accurate and that the algorithm has been effective in capturing the fold of the proteins. This has been strongly supported by the results of ProSa-web, ProQ, and Ramachandran plots.

Evaluating drug likeness and ADMET properties is crucial for therapeutic drug design, since it reduces the time and expedites drug development (Flores-Holguin et al. 2021). The evaluation of drug likeness and ADMET properties screened out 8 compounds out of 120 with favourable properties. The pharmaceutical industry commonly utilises Lipinski's rule to evaluate prospective drug candidates (Knoll et al. 2022). Remarkably, these eight compounds followed Lipinski's rule, signifying their effectiveness after oral administration. This suggested adequate absorption or penetration. The molecular weight of the screened compounds demonstrated satisfactory values, implying their favourable bioavailability characteristics. The intestinal absorption of an administered drug is a crucial aspect of drug discovery (Flores-Holguin et al. 2021). Acceptable TPSA values affirmed proper absorption of the eight compounds within the intestine (Ibrahim et al. 2020). The log S values illustrated moderate to good water solubility. Additionally, the optimal lipophilicity values (log P) of six compounds suggested effective permeability through the mycobacterial cells (Iacobino et al. 2017). Again, higher lipophilicity values of bonianic acid A and phytol suggested improved permeability and efficacy. These are well supported by their log D values.

The desirable CaCo-2 permeability of seven compounds reflected their promising membrane permeability properties (Gheidari et al. 2024). However, a slightly lower

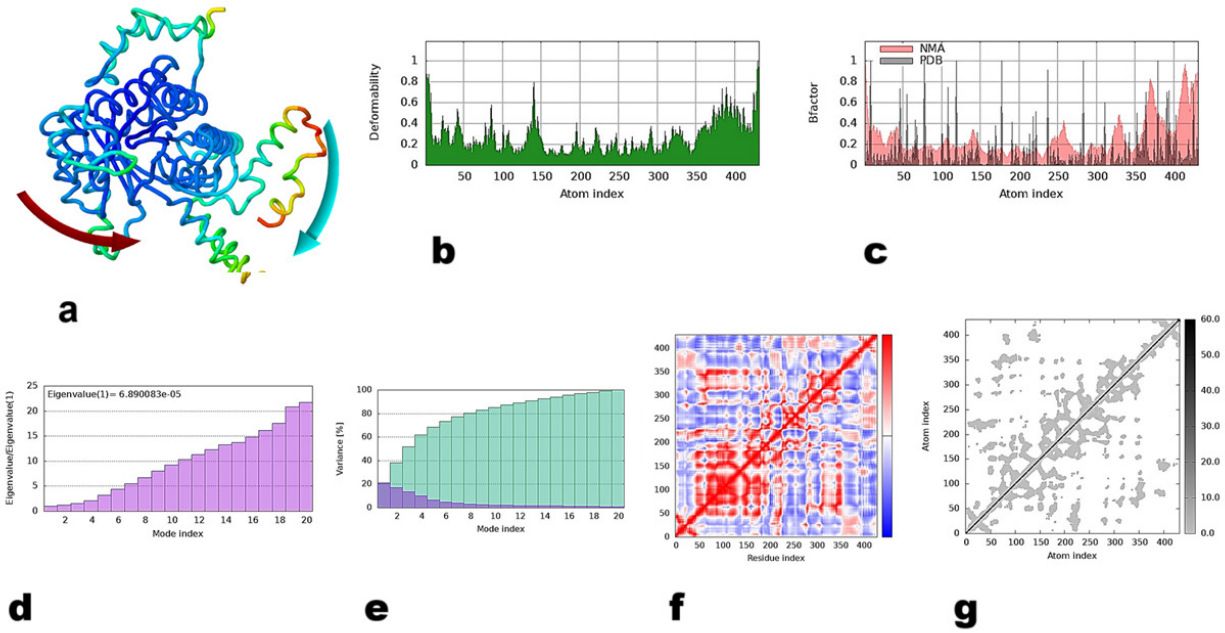

Figure 6. Normal mode analysis of the docked complex of the isocitrate lyase protein of *M. abscessus* subsp. *bolletii* BD with bisdemethoxycurcumin. a) NMA mobility; b) deformability; c) B-factor; d) eigenvalues; e) variance (purple and green colours indicate individual and cumulative variances); f) covariance map (red, white, and blue colours specify correlated, uncorrelated, and anti-correlated motions); g) elastic network. The affine arrows denote the trajectories.

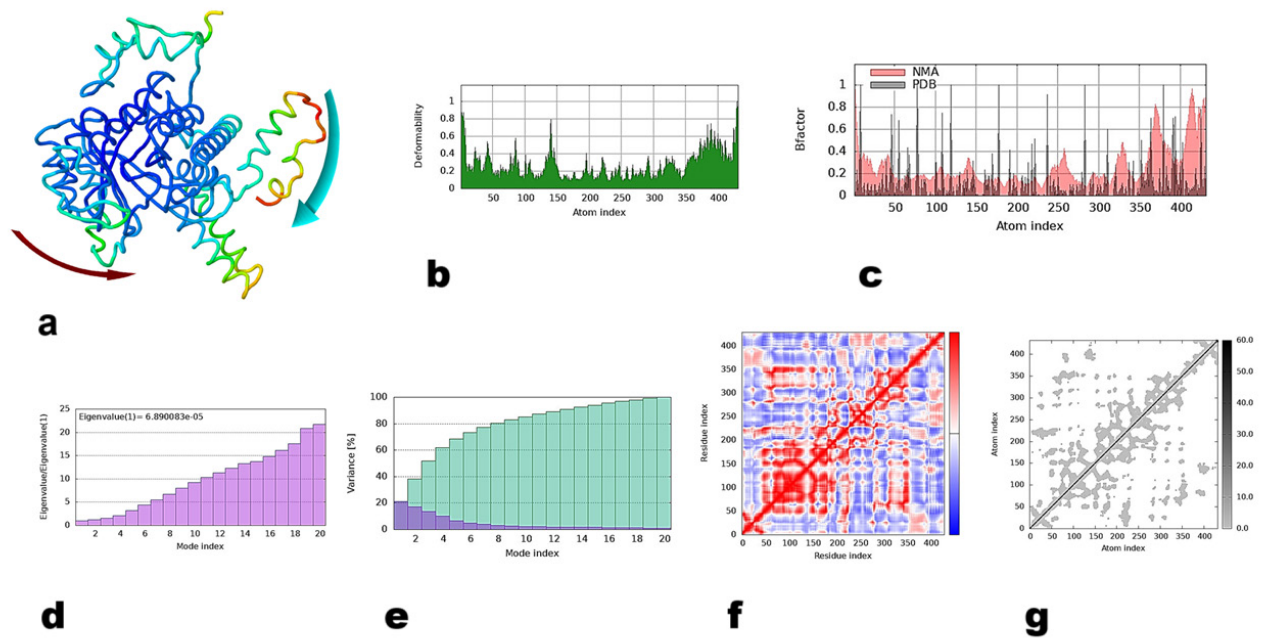

Figure 7. Normal mode analysis of the docked complex of the isocitrate lyase protein of *M. abscessus* subsp. *abscessus* ATCC 19977 with demethoxycurcumin. a) NMA mobility; b) deformability; c) B-factor; d) eigenvalues; e) variance (purple and green colours indicate individual and cumulative variances); f) covariance map (red, white, and blue colours specify correlated, uncorrelated, and anti-correlated motions); g) elastic network. The affine arrows denote the trajectories.

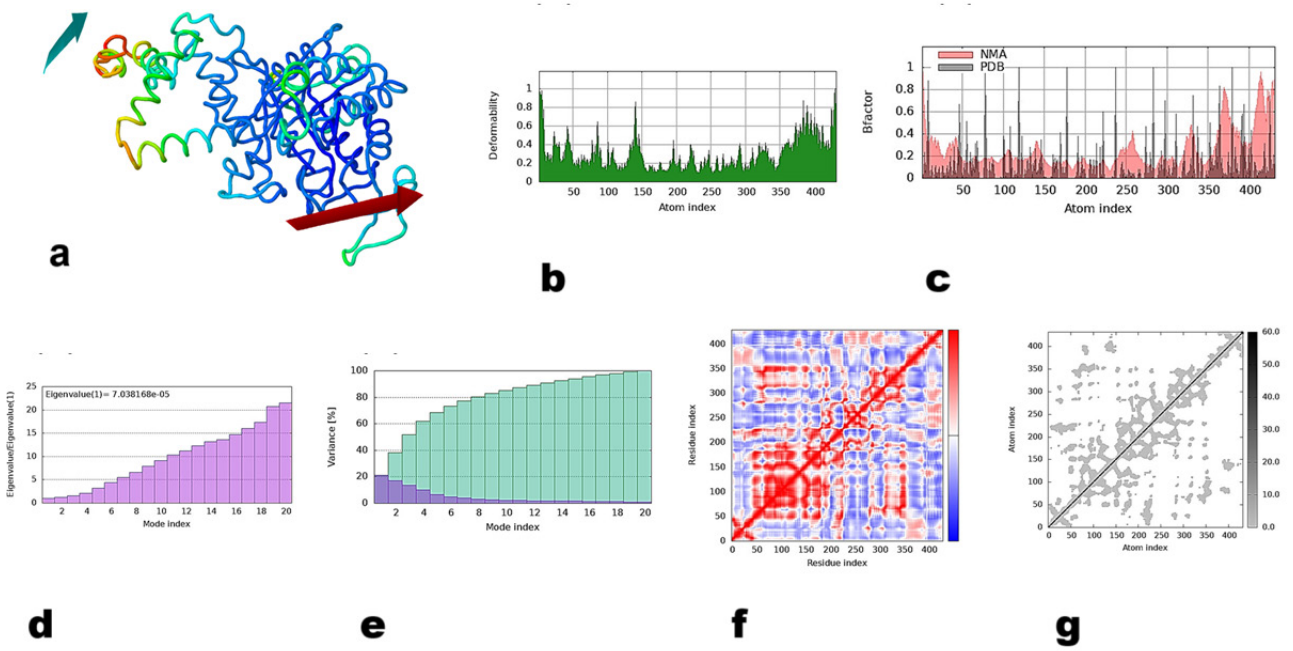

Figure 8. Normal mode analysis of the docked complex of the isocitrate lyase protein of *M. abscessus* subsp. *abscessus* ATCC 19977 with bonianic acid A. a) NMA mobility; b) deformability; c) B-factor; d) eigenvalues; e) variance (purple and green colours indicate individual and cumulative variances); f) covariance map (red, white, and blue colours specify correlated, uncorrelated, and anti-correlated motions); g) elastic network. The affine arrows denote the trajectories.

Caco-2 cell permeability of demethoxycurcumin demands improvement of its solubility. The P-glycoprotein facilitates the removal of toxins from the cells (Pires et al. 2015). This study found that some of the screened compounds were both Pgp inhibitors and substrates. It indicated their enhanced bioavailability. Conversely, phytol and bonianic acid A were not Pgp inhibitor and Pgp substrate, respectively. It meant comparatively diminished export and the probability of accumulation in the target organs. Adjusting the dosage or reducing the concentration of phytol and bonianic acid A can overcome the effect. The computed values for human intestinal absorption (HIA) indicated that all eight compounds had a tendency for successful absorption through the intestinal membrane (Gheidari et al. 2024). A study of plasma protein binding (PPB) is vital for estimating the therapeutic index of the drugs, and those with PPB values < 90% demonstrate enhanced therapeutic index (Gheidari et al. 2024). Seven compounds had optimal plasma protein binding (PPB) values, indicating a good therapeutic index, while a lower dosage of bonianic acid A would enhance its effect. Comprehending a drug's capability to cross the blood-brain barrier (BBB) is vital for minimizing side effects and toxicities (Pires et al. 2015). BBB values less than 1 for the eight compounds revealed minimal likelihood of neurotoxicity, e.g., behavioural effects, altered sensation, cognitive effects, psychosis, muscular weakness, etc. (Bangert and Hasbun 2019; Knoll et al. 2022).

The cytochrome P450 enzymes play a role in drug metabolism (Knoll et al. 2022). The analysis revealed varying conclusions regarding their inhibition by the eight compounds. Specifically, the probabilities of inhibition of CYP2C9 by bisdemethoxycurcumin and phytol, and CYP3A4 by bisdemethoxycurcumin, celahin C, and demethoxycurcumin highlighted the need for attention while jointly administering them with other antimycobacterial compounds, to avoid their accumulation (Knoll et al. 2022). Further in vitro experimentation regarding their dosage and concentration would provide valuable insights. Drug clearance occurring through hepatic and renal clearance impacts bioavailability. Results for CL_{plasma} and $T_{1/2}$ indicated that less frequent drug administration could be required, improving patient coherence and reducing the risk of drug resistance.

AMES mutagenicity is a widely employed technique to investigate the mutagenic potential of a compound (Flores-Holguin et al. 2021). Barring a moderate probability in galegin, none of the rest seven compounds was mutagenic. Additionally, neither of these eight compounds was carcinogenic. While bisdemethoxycurcumin revealed a moderate risk as a hERG blocker, adjusting the dosage may minimise the risk. That the other seven compounds

were not identified as hERG blockers signified that they did not interfere with heart rhythms. Furthermore, there was a low likelihood of having hematotoxic, nephrotoxic, hepatotoxic, and respiratory toxic properties. In contrast, phytol and galegin were identified as having strong eye corrosive and genotoxic properties. Over and above, the drug likeness and ADMET properties of these compounds appeared promising.

Molecular docking techniques have been effective in detecting optimal conformations and interactions of ligands at the binding site of target proteins (Kamel et al. 2022). Here, molecular docking studies were performed to examine the interaction of isocitrate lyase proteins with the natural products characterised by favourable drug-likeness and ADMET properties. The blind docking technique of CB-Dock2 was employed owing to the lack of prior information regarding the binding mode of these natural products with the isocitrate lyase proteins (Hetényi and van der Spoel 2006). It uncovered the binding sites and modes of the natural products by scanning the entire surface of isocitrate lyase. The observed negative and lower value of the Vina score reflected a strong binding affinity between the protein and natural products, confirming the favourable conformation of the ligands (Umesh et al. 2020; Liu et al. 2022). The docking results, including Vina scores, manifested that the screened natural products effectively fit into the active site, and establish favourable interactions with the amino acid residues of the binding sites of isocitrate lyase. In this regard, bonianic acid A, demethoxycurcumin, and bisdemethoxycurcumin demonstrated robust binding affinities. The extracellular glycans of mycobacteria assist in adhesion, immune evasion, and survival in different environments. Bonianic acid A is known to target the extracellular glycans of mycobacteria, enabling the penetration of other therapeutics into the complex mycobacterial cell wall (Truong et al. 2011). Furthermore, an earlier study of bonianic acid A, along with ergosterol peroxide, showed enhanced efficacy against mycobacteria (Truong et al. 2011). The strong binding affinity of bonianic acid A with isocitrate lyase of *M. abscessus* subsp. *bolletii* BD suggested a favourable interaction between them. Demethoxycurcumin is a promising compound possessing considerable antimycobacterial activity (Agrawal et al. 2008). Its strong binding affinity with the isocitrate lyase of *M. abscessus* subsp. *abscessus* ATCC 19977 illustrated its potential. Likewise, bisdemethoxycurcumin, a curcuminoid derivative, is antimycobacterial (Barua and Buragohain 2021) and has been known to improve the efficacy of conventional antibiotics against bacteria (Wang et al. 2020). Its favourable binding affinity with the amino acid residues of isocitrate lyase of *M. abscessus* subsp. *abscessus* ATCC 19977 indicated a prominent interaction. In summary, these three natural products are lead compounds for targeting isocitrate lyase. The outcome of molecular docking would assist future research, since it provided a foundation for the assessment of the pharmacokinetic parameters of the lead compounds in animal models.

The iMODS platform provided insights into the atomic and molecular movements of the top docked complexes. The deformability plot highlighted little distortion in the complexes. The B-factor values indicated that regions with high values are likely to be involved in conformational changes, while those with lower values constituted the structural core of the isocitrate lyase protein (Lopez-Blanco et al. 2014). Eigenvalues of the docked complexes signified stiffer regions less likely to contribute to biological motions, indicating that C alpha atoms would require additional energy for deformation (Lopez-Blanco et al. 2014; Ali et al. 2023; Pang et al. 2024), indicating stable structures. The normal mode of the docked complexes, linked to the variance plots, highlighted both individual and cumulative variances. Covariance plots facilitated understanding of how different molecular regions move relative to each other (Pang et al. 2024). The stiffer grey regions in the elastic map represented areas of restricted movement and increased structural rigidity. These are crucial for maintaining the molecular framework, since they correspond to active sites, binding pockets, or dimerisation interfaces that require stability (Lopez-Blanco et al. 2014). Unlike the white flexible regions that enable dynamic changes, the grey regions underscored minimal conformational shifts during normal mode analysis.

Conclusions

The infections caused by *M. abscessus* have resulted in diseases all over the world. Isocitrate lyase is crucial for the pathogenesis of *M. abscessus*. This study employed bioinformatics techniques to screen and design natural products targeting isocitrate lyase in the virulent and antibiotic-resistant strains of *M. abscessus*. Eight natural compounds were identified as promising candidates based on their drug-likeness and favourable ADMET properties. Active site residues were identified based on the higher binding affinity of the top compounds: bonianic acid A, demethoxycurcumin, and bisdemethoxycurcumin with isocitrate lyase. The analysis of docking interaction indicated favourable binding between these natural products and isocitrate lyase. Molecular simulations revealed the stability of the docked complexes, supporting their role in complex formation. The findings from this pilot-scale in silico analysis suggest that bonianic acid A, demethoxycurcumin, and bisdemethoxycurcumin are lead compounds that can target isocitrate lyase for treating *M. abscessus*

infections. The results from this study are likely to aid in vitro activity assays and in vivo research and may be extended to other drug-resistant and clinically important mycobacterial strains.

Acknowledgements

MK thanks the Government of West Bengal, India, for providing the SVMCM fellowship. SS thanks Ramananda College for providing the necessary infrastructure to perform the work.

References

Abrahams KA, Besra GS (2020) Mycobacterial drug discovery. RSC Med Chem 11(12):1354-1365.

Acquah KS, Gammon DW, Beukes DR (2024) South African actinobacteria: A treasure trove of novel bioactive metabolites for drug discovery. S Afr J Sci 120(1/2).

Agrawal DK, Saikia D, Tiwari R, Ojha S, Shanker K, Kumar JK, Gupta AK, Tandon S, Negi AS, Khanuja SP (2008) Demethoxycurcumin and its semisynthetic analogues as antitubercular agents. Planta Med 74(15):1828-31.

Aina SO, Rofiu MO, Olaba-Whenu OA, Olasupo IA, Adams LA, Familoni OB (2024) Drug design and in-silico study of 2-alkoxylatedquinoline-3-carbaldehyde compounds: inhibitors of *Mycobacterium tuberculosis*. Sci Afr 23: e01985.

Ali SL, Ali A, Alamri A, Baiduissenova A, Dusmagambetov M, Abduldayeva A (2023) Genomic annotation for vaccine target identification and immunoinformatics-guided multi-epitope-based vaccine design against Songling virus through screening its whole genome encoded proteins. Front Immunol 14:1284366.

Bangert MK, Hasbun R (2019) Neurological and psychiatric adverse effects of antimicrobials. CNS Drugs 33:727–753.

Baptista R, Bhowmick S, Shen J, Mur LAJ (2021) Molecular docking suggests the targets of anti-mycobacterial natural products. Molecules 26(2):475

Barua N, Buragohain AK (2021) Therapeutic potential of curcumin as an antimycobacterial agent. Biomolecules. 11(9):1278.

Başar Y, Yenigün S, Gül F, Ozen T, Demirtaş İ, Alma MH, Temel S (2024) Phytochemical profiling, molecular docking, and ADMET prediction of crude extract of *Atriplex nitens* Schkuhr for the screening of antioxidant and urease inhibitory. Int J Chem Technol 8(1):60-68.

Bosch B, DeJesus MA, Schnappinger D, Rock JM (2024) Weak links: advancing target-based drug discovery by identifying the most vulnerable targets. Ann N Y Acad Sci 1535(1):10-19.

Boshoff HI, Malhotra N, Barry CE 3rd, Oh S (2024) The antitubercular activities of natural products with fused-nitrogen-containing heterocycles. Pharmaceuticals (Basel) 17(2):211.

Bryant JM, Grogono DM, Rodriguez-Rincon D, Everall I, Brown KP, Moreno P, Verma D, Hill E, Drijkoningen J, Gilligan P, Esther CR, Noone PG, Giddings O, Bell SC, Thomson R, Wainwright CE, Coulter C, Pandey S, Wood ME, Stockwell RE, Ramsay KA, Sherrard LJ, Kidd TJ, Jabbour N, Johnson GR, Knibbs LD, Morawska L, Sly PD, Jones A, Bilton D, Laurenson I, Ruddy M, Bourke S, Bowler IC, Chapman SJ, Clayton A, Cullen M, Daniels T, Dempsey O, Denton M, Desai M, Drew RJ, Edenborough F, Evans J, Folb J, Humphrey H, Isalska B, Jensen-Fangel S, Jönsson B, Jones AM, Katzenstein TL, Lillebaek T, MacGregor G, Mayell S, Millar M, Modha D, Nash EF, O'Brien C, O'Brien D, Ohri C, Pao CS, Peckham D, Perrin F, Perry A, Pressler T, Prtak L, Qvist T, Robb A, Rodgers H, Schaffer K, Shafi N, van Ingen J, Walshaw M, Watson D, West N, Whitehouse J, Haworth CS, Harris SR, Ordway D, Parkhill J, Floto RA (2016) Emergence and spread of a human-transmissible multidrug-resistant nontuberculous mycobacterium. Science 354(6313):751–757.

Bultum LE, Tolossa GB, Kim G, Kwon O, Lee D (2022) In silico activity and ADMET profiling of phytochemicals from Ethiopian indigenous aloes using pharmacophore models. Sci Rep 12:22221.

Campillos M, Kuhn M, Gavin AC, Jensen LJ, Bork P (2008) Drug target identification using side-effect similarity. Science 321(5886):263-266.

Canales CSC, Pavan AR, Dos Santos JL, Pavan FR (2024) In silico drug design strategies for discovering novel tuberculosis therapeutics. Expert Opin Drug Discov 19(4):471-491.

Davidson RM, Hasan NA, de Moura VC, Duarte RS, Jackson M, Strong M (2013). Phylogenomics of Brazilian epidemic isolates of *Mycobacterium abscessus* subsp. *bolletii* reveals relationships of global outbreak strains. Infect Genet Evol 20:292-7.

Davidson RM, Hasan NA, Reynolds PR, Totten S, Garcia B, Levin A, Ramamoorthy P, Heifets L, Daley CL, Strong M (2014) Genome sequencing of *Mycobacterium abscessus* isolates from patients in the United States and comparisons to globally diverse clinical strains. J Clin Microbiol 52(10):3573-82.

Davidson RM (2018) A closer look at the genomic variation of geographically diverse *Mycobacterium abscessus* clones that cause human infection and disease. Front Microbiol 9:2988.

Dong J, Wang NN, Yao ZJ, Zhang L, Cheng Y, Ouyang D, Lu AP, Cao DS (2018) ADMETlab: a platform for systematic ADMET evaluation based on a comprehensively collected

ADMET database. J Cheminform 10(1):29.
Dubus E, Ijjaali I, Barberan O, Petitet F (2009) Drug repositioning using in silico compound profiling. Future Med Chem 1(9):1723-1736.
Dunn MF, Ramírez-Trujillo JA, Hernández-Lucas I (2009) Major roles of isocitrate lyase and malate synthase in bacterial and fungal pathogenesis. Microbiology (Reading) 155(Pt10):3166-3175.
Ertl P, Rohde B, Selzer P (2000) Fast calculation of molecular polar surface area as a sum of fragment-based contributions and its application to the prediction of drug transport properties. J Med Chem 43(20):3714-7.
Faïon L, Djaout K, Frita R, Pintiala C, Cantrelle FX, Moune M, Vandeputte A, Bourbiaux K, Piveteau C, Herledan A, Biela A, Leroux F, Kremer L, Blaise M, Tanina A, Wintjens R, Hanoulle X, Déprez B, Willand N, Baulard AR, Flipo M (2020) Discovery of the first *Mycobacterium tuberculosis* MabA (FabG1) inhibitors through a fragment-based screening. Eur J Med Chem 200:112440.
Flores-Holguín N, Frau J, Glossman-Mitnik D (2021) In silico pharmacokinetics, ADMET study and conceptual DFT analysis of two plant cyclopeptides isolated from Rosaceae as a computational peptidology approach. Front Chem 9:708364.
Fu L, Shi S, Yi J, Wang N, He Y, Wu Z, Peng J, Deng Y, Wang W, Wu C, Lyu A, Zeng X, Zhao W, Hou T, Cao D (2024) ADMETlab 3.0: an updated comprehensive online ADMET prediction platform enhanced with broader coverage, improved performance, API functionality and decision support. Nucleic Acids Res 52(W1): W422- W431.
Gagare S, Patil P, Jain A (2024) Natural product-inspired strategies towards the discovery of novel bioactive molecules. Futur J Pharm Sci 10:55.
Ganapathy US, Dick T (2022) Why matter matters: fast-tracking *Mycobacterium abscessus* drug discovery. Molecules 27(20):6948.
Gasteiger E, Hoogland C, Gattiker A, Duvaud S, Wilkins MR, Appel RD, Bairoch A (2005) Protein identification and analysis tools on the ExPASy server. In Walker JM, Ed., The Proteomics Protocols Handbook. Humana Press, Totowa, 571–607.
Gheidari D, Mehrdad M, Karimelahi Z (2024) Virtual screening, ADMET prediction, molecular docking, and dynamic simulation studies of natural products as BACE1 inhibitors for the management of Alzheimer's disease. Sci Rep 14(1):26431.
Hetényi C, van der Spoel D (2006). Blind docking of drug-sized compounds to proteins with up to a thousand residues. FEBS Lett 580(5):1447-1450.
Iacobino A, Piccaro G, Giannoni F, Mustazzolu A, Fattorini L (2017) Fighting tuberculosis by drugs targeting nonreplicating *Mycobacterium tuberculosis* bacilli. Int J Mycobacteriol 6:213.
Ibekwe NN and Ameh SJ (2014) Plant natural product research in tuberculosis drug discovery and development: A situation report with focus on Nigerian biodiversity. Afr J Biotechnol 13(23):2307-2320.
Ibrahim ZY, Uzairu A, Shallangwa G, Abechi S (2020) Molecular docking studies, drug-likeness and in-silico ADMET prediction of some novel β-Amino alcohol grafted 1,4,5-trisubstituted 1,2,3-triazoles derivatives as elevators of p53 protein levels. Sci Afr 10: e00570.
Igarashi M, Ishizaki Y, Takahashi Y (2018) New antituberculous drugs derived from natural products: current perspectives and issues in antituberculous drug development. J Antibiot (Tokyo). 71:15–25.
Jaiswal N, Kumar A (2023) A soft-computation hybrid method for search of the antibiotic-resistant gene in *Mycobacterium tuberculosis* for promising drug target identification and antimycobacterial lead discovery. Bioinform Adv 3(1): vbad090.
Jarand J, Levin A, Zhang L, Huitt G, Mitchell JD, Daley CL (2011) Clinical and microbiological outcomes in patients receiving treatment for *Mycobacterium abscessus* pulmonary disease. Clin Infect Dis 52(5):565–571.
Johansen MD, Herrmann JL, Kremer L (2020) Non-tuberculous mycobacteria and the rise of *Mycobacterium abscessus*. Nat Rev Microbiol 18(7):392–407.
Junk L, Schmiedel VM, Guha S, Fischel K, Greb P, Vill K, Krisilia V, van Geelen L, Rumpel K, Kaur P, Krishnamurthy RV, Narayanan S, Shandil RK, Singh M, Kofink C, Mantoulidis A, Biber P, Gmaschitz G, Kazmaier U, Meinhart A, Leodolter J, Hoi D, Junker S, Morreale FE, Clausen T, Kalscheuer R, Weinstabl H, Boehmelt G (2024) Homo-BacPROTAC-induced degradation of ClpC1 as a strategy against drug-resistant mycobacteria. Nat Commun 15(1):2005.
Kalera K, Liu R, Lim J, Pathirage R, Swanson DH, Johnson UG, Stothard AI, Lee JJ, Poston AW, Woodruff PJ, Ronning DR, Eoh H, Swarts BM (2024) Targeting *Mycobacterium tuberculosis* persistence through inhibition of the trehalose catalytic shift. ACS Infect Dis 10(4):1391-1404.
Kamel MS, Belal A, Aboelez MO, Shokr EK, Abdel-Ghany H, Mansour HS, Shawky AM, El-Remaily MAEAAA (2022) Microwave-assisted synthesis, biological activity evaluation, molecular docking, and ADMET studies of some novel pyrrole [2,3-b] pyrrole derivatives. Molecules 27(7): 2061.
Karmakar M, Sur S (2025) Unlocking the *Mycobacteroides abscessus* pan-genome using computational tools: insights into evolutionary dynamics and lifestyle. Antonie Van Leeuwenhoek 118(1):30.
Kim S, Thiessen PA, Bolton EE, Chen J, Fu G, Gindulyte A, Han L, He J, He S, Shoemaker BA, Wang J, Yu B, Zhang J, Bryant SH (2016). PubChem substance and compound databases. Nucleic Acids Res 44(D1): D1202-13.

Knoll KE, van der Walt MM, Loots DT (2022) In Silico drug discovery strategies identified ADMET properties of decoquinate RMB041 and its potential drug targets against *Mycobacterium tuberculosis*. Microbiol Spectr 10(2): e0231521.

Kumar S, Sahu P, Jena L (2019) An *In silico* approach to identify potential inhibitors against multiple drug targets of *Mycobacterium tuberculosis*. Int J Mycobacteriol 8(3):252-261.

Kumar V, Shankar G, Akhter Y (2023) Deciphering drug discovery and microbial pathogenesis research in tuberculosis during the two decades of postgenomic era using entity mining approach. Arch Microbiol 206(1):46.

Kumpf O, Gürtler K, Sur S, Parvin M, Zerbe LK, Eckert JK, Weber ANR, Oh DY, Lundvall L, Hamann L, Schumann RR (2021) A genetic variation of lipopolysaccharide binding protein affects the inflammatory response and is associated with improved outcome during sepsis. Immunohorizons 5(12):972-982.

Lee YV, Wahab HA, Choong YS (2015) Potential inhibitors for isocitrate lyase of *Mycobacterium tuberculosis* and non-*M. tuberculosis*: a summary. Biomed Res Int 2015:895453.

Liu Y, Yang X, Gan J, Chen S, Xiao ZX, Cao Y (2022) CB-Dock2: improved protein-ligand blind docking by integrating cavity detection, docking and homologous template fitting. Nucleic Acids Res 50(W1): W159- W164.

Lipinski CA (2004) Lead- and drug-like compounds: the rule-of-five revolution. Drug Discov Today Technol 1(4):337-41.

López-Blanco JR, Aliaga JI, Quintana-Ortí ES, Chacón P (2014) iMODS: internal coordinates normal mode analysis server. Nucleic Acids Res 42(Web Server issue): W271-W276.

Mandal S, Kar NR, Jain AV, Yadav P (2024) Natural products as sources of drug discovery: exploration, optimisation, and translation into clinical practice. Afr J Bio Sci 6(9):2486-2504.

McGuffin LJ, Bryson K, Jones DT (2000) The PSIPRED protein structure prediction server. Bioinformatics 16(4):404-405.

Mougari F, Raskine L, Ferroni A, Marcon E, Sermet-Gaudelus I, Veziris N, Heym B, Gaillard JL, Nassif X, Cambau E (2014) Clonal relationship and differentiation among *Mycobacterium abscessus* isolates as determined using the semiautomated repetitive extragenic palindromic sequence PCR-Based diversiLab system. J Clin Microbiol 52(6):1969–1977.

Newman DJ, Cragg GM (2020) Natural products as sources of new drugs over the nearly four decades from 01/1981 to 09/2019. J Nat Prod 83(3):770-803.

Nguta JM, Appiah-Opong R, Nyarko AK, Yeboah-Manu D, Addo PG (2015) Current perspectives in drug discovery against tuberculosis from natural products. Int J Mycobacteriol 4(3):165-83.

Nyambo K, Tapfuma KI, Adu-Amankwaah F, Julius L, Baatjies L, Niang IS, Smith L, Govender KK, Ngxande M, Watson DJ, Wiesner L, Mavumengwana V (2024) Molecular docking, molecular dynamics simulations and binding free energy studies of interactions between *Mycobacterium tuberculosis* Pks13, PknG and bioactive constituents of extremophilic bacteria. Sci Rep 14(1):6794.

Pang F, Long Q, Liang S (2024) Designing a multi-epitope subunit vaccine against Orf virus using molecular docking and molecular dynamics. Virulence 15(1):2398171.

Pires DE, Blundell TL, Ascher DB (2015) pkCSM: predicting small-molecule pharmacokinetic and toxicity properties using graph-based signatures. J Med Chem 58(9):4066-72.

Ripoll F, Pasek S, Schenowitz C, Dossat C, Barbe V, Rottman M, Macheras E, Heym B, Herrmann JL, Daffé M, Brosch R, Risler JL, Gaillard JL (2009) Non mycobacterial virulence genes in the genome of the emerging pathogen *Mycobacterium abscessus*. PLoS ONE 4(6): e5660.

Sassetti CM, Rubin EJ (2003) Genetic requirements for mycobacterial survival during infection. Proc Natl Acad Sci U S A 100(22):12989-12994.

Shahab M, Danial M, Duan X, Khan T, Liang C, Gao H, Chen M, Wang D, Zheng G (2024) Machine learning-based drug design for identification of thymidylate kinase inhibitors as a potential anti-*Mycobacterium tuberculosis*. J Biomol Struct Dyn 42(8):3874-3886.

Shyam M, Kumar S, Singh V (2024) Unlocking opportunities for *Mycobacterium leprae* and *Mycobacterium ulcerans*. ACS Infect Dis 10(2):251-269.

Sirichoat A, Kham-Ngam I, Kaewprasert O, Ananta P, Wisetsai A, Lekphrom R, Faksri K (2021) Assessment of antimycobacterial activities of pure compounds extracted from Thai medicinal plants against clarithromycin-resistant *Mycobacterium abscessus*. Peer J 9: e12391.

Smiejkowska N, Oorts L, Van Calster K, De Vooght L, Geens R, Mattelaer H-P, Augustyns K, Strelkov SV, Lamprecht D, Temmerman K, Sterckx YG-J, Cappoen D, Cos P (2024) A high-throughput target-based screening approach for the identification and assessment of *Mycobacterium tuberculosis* mycothione reductase inhibitors. Microbiol Spectr 12(3):e0372323.

Soni J, Sinha S, Pandey R (2024) Understanding bacterial pathogenicity: a closer look at the journey of harmful microbes. Front Microbiol 15:1370818.

Sullivan JR, Yao J, Courtine C, Lupien A, Herrmann J, Müller R, Behr MA (2022) Natural Products lysobactin and sorangicin A show in vitro activity against *Mycobacterium abscessus* complex. Microbiol Spectr 10(6): e0267222.

Sur S, Patra T, Karmakar M, Banerjee A (2023) *Mycobacterium abscessus*: insights from a bioinformatic perspective. Crit Rev Microbiol 49(4):499–514.

Thada S, Burkert S, Sivangala R, Hussain A, Sur S, Dittrich

N, Conrad ML, Slevogt H, Latha Gaddam S, Schumann RR (2020) A SNP upstream of the cyclic GMP-AMP synthase (cGAS) gene protects from relapse and extrapulmonary TB and relates to BCG vaccination status in an Indian cohort. Genes Immun 21(1):13-26.

Truong NB, Pham CV, Doan HT, Nguyen HV, Nguyen CM, Nguyen HT, Zhang HJ, Fong HH, Franzblau SG, Soejarto DD, Chau MV (2011) Antituberculosis cycloartane triterpenoids from *Radermachera boniana*. J Nat Prod 74(5):1318-22.

Umesh HR, Ramesh KV, Devaraju KS (2020) Molecular docking studies of phytochemicals against trehalose–6–phosphate phosphatases of pathogenic microbes. Beni-Suef Univ J Basic Appl Sci 9:5.

Veber DF, Johnson SR, Cheng HY, Smith BR, Ward KW, Kopple KD (2002) Molecular properties that influence the oral bioavailability of drug candidates. J Med Chem 45(12):2615-23.

Vereecke D, Cornelis K, Temmerman W, Jaziri M, Van Montagu M, Holsters M, Goethals K (2002) Chromosomal locus that affects pathogenicity of *Rhodococcus fascians*. J Bacteriol 184(4):1112-1120.

Wallner B, Elofsson A (2003) Can correct protein models be identified? Protein Sci 12(5):1073-1086.

Wang S, Kim MC, Kang OH, Kwon DY (2020) The mechanism of bisdemethoxycurcumin enhances conventional antibiotics against methicillin-resistant *Staphylococcus aureus*. Int J Mol Sci 21(21):7945.

Wayne LG, Lin KY (1982) Glyoxylate metabolism and adaptation of *Mycobacterium tuberculosis* to survival under anaerobic conditions. Infect Immun 37(3):1042-1049.

Wiederstein M, Sippl MJ (2007) ProSA-web: interactive web service for the recognition of errors in three-dimensional structures of proteins. Nucleic Acids Res 35 (Web Server issue): W407-10.

Zhang L, Lin TY, Liu WT, Ling F (2024) Toward characterizing environmental sources of non-tuberculous mycobacteria (NTM) at the species level: a tutorial review of NTM phylogeny and phylogenetic classification. ACS Environ Au 4(3):127–141.

Zheng Y, Jiang X, Gao F, Song J, Sun J, Wang L, Sun X, Lu Z, Zhang H (2014) Identification of plant-derived natural products as potential inhibitors of the *Mycobacterium tuberculosis* proteasome. BMC Complement Altern Med 14:400.